Journal of Physics: Conference Series **589** (2015) 012013 doi:10.1088/1742-6596/589/1/012013

High-p_T hadrons in pA and AA collisions: Impact of energy conservation

B.Z. Kopeliovich[1], J. Nemchik[2,3], I.K. Potashnikova[1] and Ivàn Schmidt[1]

[1]Departamento de Física, Universidad Técnica Federico Santa María;
Centro Científico-Tecnológico de Valparaíso, Avda. España 1680, Valparaíso, Chile
[2] Czech Technical University in Prague, FNSPE, Břehová 7, 11519 Prague, Czech Republic
[3] Institute of Experimental Physics SAS, Watsonova 47, 04001 Košice, Slovakia

E-mail: boris.kopeliovich@usm.cl

Abstract. The Cronin effect, which is nuclear enhancement of high-p_T hadron production in pA collisions was successfully predicted prior the measurements at RHIC and LHC. The restrictions imposed by energy conservation lead to spectacular effects. Energy deficit becomes an issue for hadron production in pA collisions at large x_L and/or large x_T towards the kinematic bounds $x_{L,T} = 1$. It leads to a suppression, which has been indeed observed for hadrons produced at forward rapidities and large p_T. Intensive energy dissipation via gluon radiation by a highly virtual parton produced with large p_T, makes impossible this process to continue long. Color neutralization and creation of a colorless dipole must occur promptly. When this happens inside a hot medium created in AA collisions, attenuation of dipoles, rather than induced energy loss, becomes a dominant mechanism for suppression of high-p_T hadrons.

1. pA collisions: Cronin effect

High-p_T hadrons can be produced coherently from multiple interactions in nuclei at very high energies (LHC), but not at low energies of fixed target experiments. Correspondingly, the mechanisms for the Cronin enhancement are different. Within the parton model high-p_T hadron production results from hard scattering of the partons, which belong to the colliding hadrons, $1 + 2 \to 3 + 4$. This process looks quite differently in the rest frame of the target, where the produced partons 3 and 4 pre-exist as a high-p_T fluctuation inside the incident hadron. Such a duality in the interpretation of the process is illustrated in Fig. 1. The parton model description illustrated in the left part of Fig. 1, is more suitable at low energy where the coherence time of radiation (see below) is short. The results of description of low energy data from fixed target experiments are depicted in Fig. 2. The calculations [1] are parameter free, since the magnitude of broadening is calculated (see details in [1, 2]).

At higher energies, if both x_1 and x_2 are sufficiently small, one can assume that the colliding partons 1 and 2 are gluons. The initial gluon 1 can fluctuate as is depicted in Fig. 1 (right) either as $g \to gg$, or $g \to q\bar{q}$. The latter is a higher order correction within the leading $\log(s)$ dynamics, since misses the $\ln(s)$ enhancement factor, which is contained in the $g_1 \to g_3 g_4$ term due to the integration $d\alpha/\alpha$, where $\alpha = p_+^{(3)}/p_+^{(1)}$ is the fractional light-cone momentum of the produced gluon. Such an α-distribution of radiated gluons results in a small value of the mean fractional momentum $\langle\alpha\rangle \sim 1/\ln(s) \ll 1$, neglected in what follows.

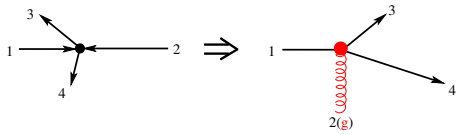

Figure 1. Production of a high-p_T parton in the c.m. frame (left) and in the rest frame of the target (right).

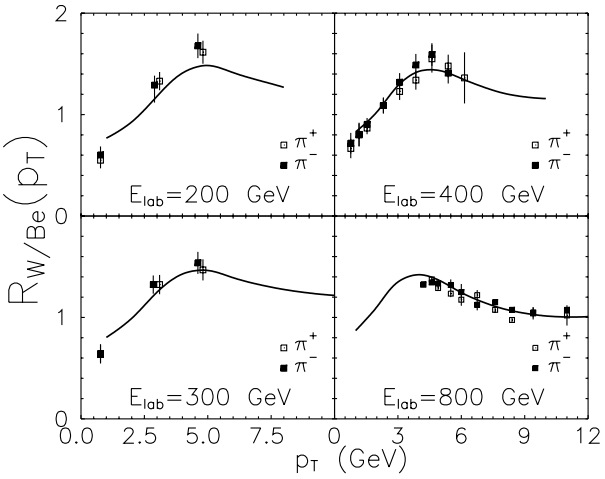

Figure 2. Fractional energy loss by a quark with different initial energies in vacuum vs path length L.

The cross section of parton 3 production integrated over the phase space of parton 4 can be expressed in terms of the interaction cross section of a dipole consisted of partons 3, 4 and $\bar{1}$, $\sigma_{\bar{1}23}(\vec{r}_{13},\vec{r}_{14})$, where $\vec{r}_{ij}$ is the transverse separation between partons i and j [3]. These distances are kinematically related, $r_{13}=(1-\alpha)r_{34}$, $r_{14}=\alpha r_{34}$.

The cross section of gluon radiation with transverse momentum k_T and rapidity y on nucleon, or nuclear targets can be represented within the dipole approach as, [3, 4, 1],

$$\frac{d\sigma^{N(A)}_{g\to 2g}(\alpha,x_2)}{d^2k_T\,dy}=\int d^2r d^2r'\,e^{i\vec{k}_T(\vec{r}-\vec{r}')}\Big\langle\Psi^\dagger_{gg}(\vec{r},\alpha)\Psi_{gg}(\vec{r}',\alpha)\Big\rangle\,\Sigma^{N(A)}_{3g}(\vec{r},\vec{r}',\alpha,x_2) \tag{1}$$

Here $\vec{r}\equiv\vec{r}_{34}$ is the transverse separation between the produced gluons g_3 and g_4; $\vec{r}'$ corresponds to the conjugated amplitude. We rely here on the high-energy approximation of small $\alpha\ll 1$, as was commented above. Correspondingly, the combination $\Sigma_{3g}(\vec{r},\vec{r}')$ of the dipole cross sections, which depends on the target, a nucleon or a nucleus, has the form [3, 4],

$$\Sigma^{N(A)}_{3g}(\vec{r},\vec{r}',\alpha)=\sigma^{N(A)}_{3g}(r,\alpha)+\sigma^{N(A)}_{3g}(r',\alpha)-\sigma^{N(A)}_{3g}(\vec{r}-\vec{r}',\alpha); \tag{2}$$

where

$$\sigma^{A}_{3g}(r,\alpha)=2\int d^2b\left[1-e^{-\frac{1}{2}\sigma^{N}_{3g}(r,\alpha)T_A(b)}\right]. \tag{3}$$

The 3-gluon ($g_1g_2g_3$) dipole cross section is related to the quark-antiquark dipole cross section on a nucleon, known well from phenomenology,

$$\sigma^{N}_{3g}(r,\alpha)=\frac{9}{8}\Big\{\sigma_{\bar{q}q}(r)+\sigma_{\bar{q}q}(\alpha r)+\sigma_{\bar{q}q}[(1-\alpha)r]\Big\}\,. \tag{4}$$

All dipole cross sections also depend implicitly on x_2, which is defined later. The impact parameter dependent nuclear thickness function $T_A(b)=\int_{-\infty}^{\infty}dz\,\rho_A(b,z)$ is a result of integration of the nuclear density along the gluon trajectory.

We should remind that we consider here only two Fock components of the physical gluon: (i) just a single gluon, and (ii) two gluons. As a result of interaction, a new final state can be produced (e.g. $g+N\to 2g+X$) only due to the difference between the interactions amplitudes of these two Fock states. The difference has a form of a three-body cross section, this is why

Eqs. (2)-(3) contain the artificial three-gluon dipole cross section, although only one or two gluons interact with the target.

The light-cone distribution function for a 2-gluon fluctuation $g \to 2g$ in Eq. (1) in the limit of small α has the form [4],

$$\Psi_{gg}(\vec{r},\alpha) = \frac{\sqrt{8\alpha_s}}{\pi\, r^2}\, \exp\left[-\frac{r^2}{2\, r_0^2}\right]\, \Big[\alpha(\vec{e}_1^{\,*}\cdot\vec{e})(\vec{e}_2^{\,*}\cdot\vec{r})+(1-\alpha)(\vec{e}_2^{\,*}\cdot\vec{e})(\vec{e}_1^{\,*}\cdot\vec{r})-\alpha(1-\alpha)(\vec{e}_1^{\,*}\cdot\vec{e}_2^{\,*})(\vec{e}\cdot\vec{r})\Big], \quad (5)$$

where $\vec{e}_i$ is the polarization vector of the gluon g_i participating in the process. The parameter $r_0 = 0.3\,\mathrm{fm}$ characterizes the strength of the nonperturbative interaction of gluons. There are many experimental [5] and theoretical [6] evidences that the mean gluon separation is short.

Eventually, the cross section of inclusive hadron production in pp or pA collision can be presented as a convolution of (1) with the gluon distribution function in the projectile proton and with the gluon fragmentation function,

$$\frac{d^2\sigma(pN(A)\to hX)}{d^2p_T\, dy} = \int\limits_{z_{min}}^{1} \frac{dz}{z^2}\, D_{h/g}(z,k_T^2) \int\limits_{x_{min}}^{1} dx_1\, g(x_1,k_T^2) \frac{d^2\sigma_{g\to 2g}^{N(A)}(\alpha,x_2)}{d^2k_T\, dy}. \quad (6)$$

Here $z_{min} = (p_T/\sqrt{s})\, e^y$; $x_{min} = z_{min}/z$; $k_T = p_T/z$. The scale for the gluon distribution and fragmentation function is imposed by gluon transverse momentum k_T. In this integral the fractional momentum of the gluon fragmenting into the detected hadron with rapidity y is related to other variables as,

$$\alpha \equiv \frac{p_+^{(3)}}{p_+^{(1)}} = \frac{p_T\, e^y}{x_1 z\sqrt{s}} = \frac{x_{min}}{x_1}. \quad (7)$$

As far as α is fixed, the value of x_2 is known as well,

$$x_2 = \frac{p_T^2}{x_1 z^2\, \alpha(1-\alpha)s} \approx \frac{p_T}{z\sqrt{s}}\, e^{-y}. \quad (8)$$

1.1. Cronin effect at RHIC: predicted and observed

The ratio of the cross sections Eq. (6) on nuclei to nucleon predicted in [1] for $\sqrt{s} = 200\,\mathrm{GeV}$ at the mid rapidity is plotted in Fig. 3 as function of p_T by dotted curve. The predicted magnitude of the nuclear enhancement was OK, but the shape of p_T-dependence was not.

The employed unintegrated gluon density proposed by Golec-Biernat and Wüsthoff (GBW) [7] peaks at too small p_T. Currently available a more realistic parametrization, for the unintegrated gluon distribution proposed later by Kimber, Martin and Ryskin (KMR) [8, 9] improves the shape. Since no other modifications was made in the computing code, the result still has the status of prediction.

Notice, that [1] was the only successful prediction at the energies of RHIC (e.g. compare with [10]).

1.2. Cronin effect at LHC

The new feature of nuclear effects at the energies of LHC is gluon shadowing, which is a negligibly small correction at RHIC. Gluon shadowing in nuclei is a part of the Gribov inelastic corrections [11] related to the triple-Pomeron term in diffraction. The expected value of the Pomeron-proton cross section is $\sigma_{tot}^{I\!Pp} \sim 50\,\mathrm{mb}$, while measured in single diffraction to large invariant masses turns out to be $\sigma_{tot}^{I\!Pp} < 2\,\mathrm{mb}$! Smallness of the diffractive cross section means weakness of gluon shadowing. In terms of pQCD this shows a suppression of diffractive gluon radiation, which can only be related to smallness of gluonic dipoles ($r_0 = 0.3\,\mathrm{fm}$ in Eq. (5)).

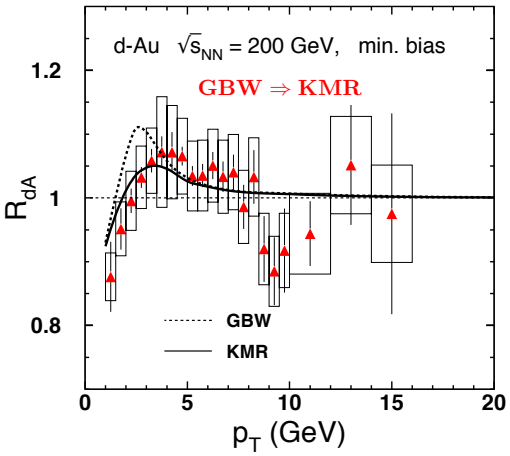

Figure 3. The nuclear to proton ratio R_{dA} as function of p_T. Dashed and solid curves show the predictions made with the GBW [7] and KMR [8, 9] parametrizations for the unintegrated gluon density. Data are from [12].

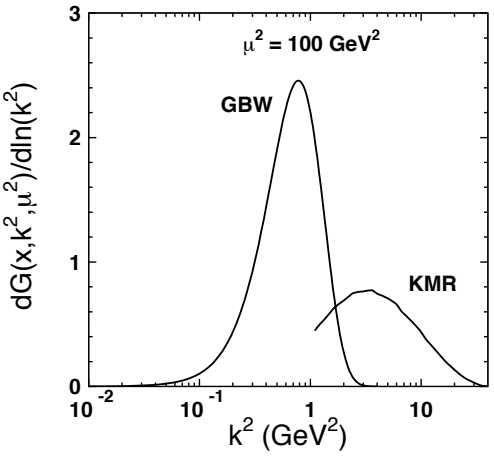

Figure 4. The k^2-dependence of the unintegrated gluon density with the GBW [7] and KMR [8, 9] parametrizations.

Gluon shadowing in DIS corresponds to inclusion of the higher Fock components of the photon, $\gamma^* \to \bar{q}q+g+...$, [4]. Although gluons do not participate in electromagnetic interactions, The gluon PDF is probed by DIS via the DGLAP evolution for the Q^2 dependence of $F_2(x, Q^2)$. So far only the NMC experiment managed to detect a variation of the nuclear PDF with Q^2. However, the data are not sensitive to gluon shadowing (at least in the leading order).

As far as the light-cone distribution function for gluons, Eq. (5), is fixed by diffraction data, the magnitude of gluon shadowing can ve evaluated theoretically [4]. The predictions made in [1] with the cross sections Eq. (6) for $\sqrt{s} = 5\,\text{TeV}$ and the mid rapidity are plotted in Fig. 5 by dotted curve in comparison with data from ALICE experiment [13]. Gluon shadowing, calculated in [4] brings $R_{pA}(p_T)$ down, as is shown by the solid curve.

Similar to the comparison done above for the RHIC data (Fig. 3), the magnitude of the Cronin enhancement is predicted correctly, but the shape of the p_T-dependence does not look correct. Again, the GBW parametrization used in [1] nowadays could be replaced by more realistic KMR form [8, 9] (see Fig. 4). This results in a considerable shift of the maximum to larger p_T, as is shown in Fig. 6. At the same time, the theoretical calculation of gluon shadowing [4] also contains considerable uncertainties. If one applies the nuclear gluon PDF extracted from data in the next-to-leading order analysis by De Florian and Sassot (DS) [14], the results seem to agree with data pretty well, both for shape and magnitude.

All these modifications demonstrate the range of theoretical uncertainties of the prediction made in citecronin-prl for the Cronin effect at the LHC energies. The modified curves still have the status of prediction, because no modification in the calculation was done, except using updated more realistic parametrizations for the phenomenological functions extracted from other reactions.

Notice that the other predictions made recently for the Cronin effect at LHC disagree with the data (see references and comparison with data in [15]).

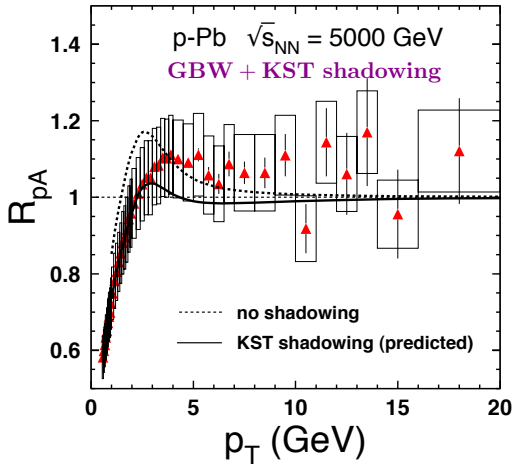

Figure 5. Data for R_{pA} from the ALICE experiment [13] at $\sqrt{s} = 5$ TeV in comparison with predictions made in [1]. Dashed and solid curves show the results calculated without and with gluon shadowing [4].

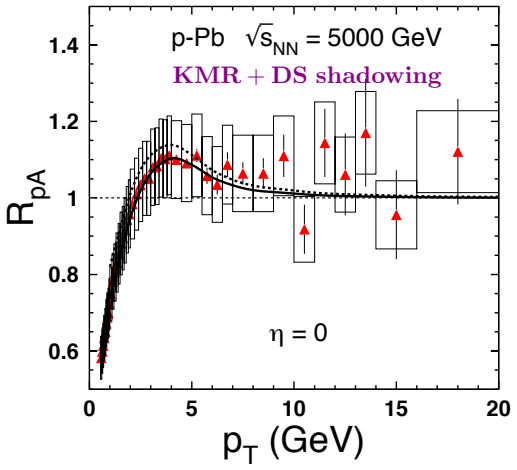

Figure 6. The same as in FIg. 5, but the calulations are performed with the KMR [8, 9] parametrization for the unintegrated gluon density. DS gluon shadowing extracted from data [14].

2. Energy deficit at forward rapidities

Multiple interactions of the projectile hadron and its debris propagating through the nucleus should cause a dissipation of energy. This intuitive expectation is supported by consideration of the Fock state decomposition. The projectile hadron can be expanded over different states which are the fluctuations of this hadron. In the limit of infinite momentum frame those fluctuations live forever. One can probe the Fock state expansion by interaction with a target. The interaction modifies the weights of the Fock states, some interact stronger, some weaker.

In each Fock component the hadron momentum is shared by the constituents, and the momentum distribution depends on their multiplicity: the more constituents are involved, the smaller is the mean energy per a constituent parton, i.e. the softer is the fractional energy distribution of a leading parton. So on a nuclear target the projectile parton distribution falls at $x \to 1$ steeper than on a proton.

In the case of a hard reaction on a nucleus, this softening of the projectile parton momentum distribution can be viewed as an effective loss of energy of the leading parton in the nuclear medium, because the initial state multiple interactions enhance the weight factors for higher Fock states in the projectile hadron. Those components with large number of constituents have a tough energy sharing, so the mean energy of the leading parton decreases compared to lower Fock states, which dominate the hard reaction on a proton target. Such a reduction of the mean energy of the leading parton can be treated as an effective energy loss, which is proportional to the initial hadron energy.

The corresponded suppression factor for each of multiple interactions was evaluated in [16], $S(\xi) \approx 1 - \xi$, where $\xi = \sqrt{x_L^2 + x_T^2}$, and $x_L = 2p_L/\sqrt{s}$; $x_T = 2p_T/\sqrt{s}$. This factor leads to a suppression of the cross section of high-p_T hadron production at forward rapidities. The results of parameter-free calculations performed in [16] depicted in Fig. 7 well agree with data from the BRAHMS [17] and STAR [18] experiments.

Notice that the alternative interpretation [20] of the suppression observed at forward rapidities is based on the effect of coherence (color glass condensate (CGC)). This effect should disappear at lower energies, because $x \propto 1/\sqrt{s}$ rises. Having no other contributing to the suppression

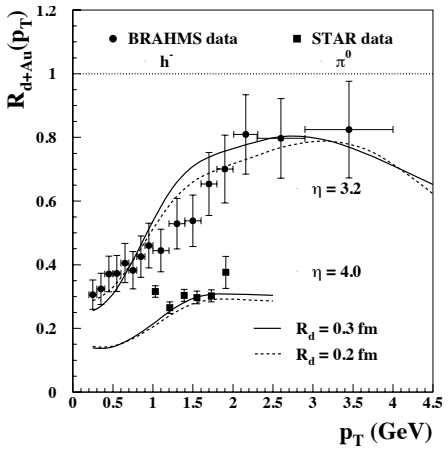

Figure 7. The nuclear ration $R_{dA}(p_T)$ measured for negative charged hadrons produced with pseudo-rapidity $\eta = 3.2$ [17] and for neutral pion produced with $\eta = 4$ [18] in dA collisions at $\sqrt{s} = 200\,\mathrm{GeV}$. The curves show the results of parameter-free calculations done in [16, 19]. Solid and dashed curves correspond to different diquark radiuses.

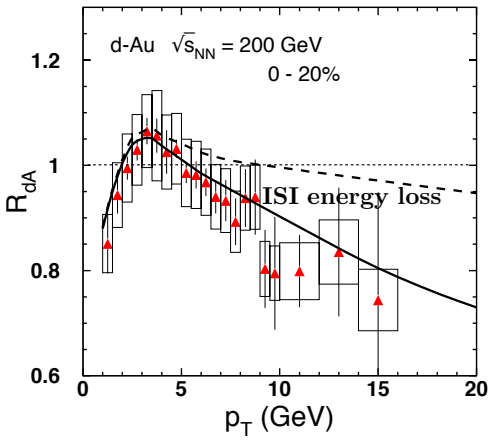

Figure 8. Nuclear ratio $R_{dA}(p_T)$ for neutral pion production in dA central collisions at $\sqrt{s} = 200\,\mathrm{GeV}$ measured in [12]. The dashed curve includes only isotopic effect (deutron vs proton), while the solid curve includes also the initial state energy loss (see the text).

observed by BRAHMS, but only CGC, one should expect no suppression at forward rapidities at lower energies. On the other hand, the suppression caused by energy deficit scales in Feynman x_F and should exist at any energy. Thus lowering the collision energy would be a sensitive test for the models. The NA49 experiment at SPS has performed measurements [21] similar to BRAHMS, but at much lower energy, where the value of x_2 is two orders of magnitude larger than in the BRAHMS data. The results show that the effect of suppression at forward rapidities is still there.

Another test of the mechanisms can be performed at large x_T. In this case no coherence effects are possible, while the value of ξ is considerable and the energy deficit should lead to a suppression at large x_T similar to what was observed at large x_L. The predictions of Ref. [19] at $\sqrt{s} = 200\,\mathrm{GeV}$ and mid rapidity are confirmed by data for central dA collisions with large p_T, as is shown in Fig. 8. No alternative explanation has been proposed so far.

3. High-p_T hadrons from AA collisions

3.1. Hard parton collisions

Parton scattering with a high transverse momentum p_T leads to formation of four cones of gluon radiation: (i) the color field of the colliding partons is shaken off in forward and backward directions; (ii) the scattered partons carry no field up to transverse momenta $k_T < p_T$ ($\vec{k}_T$ is normal to the jet direction $\vec{p}_T$), so the final state partons are regenerating the lost color field by radiating gluons and forming the up-down jets, as is illustrated in Fig. 9.

The coherence length/time of radiation of a gluon carrying fractional light-cone momentum x reads,

$$l_c = \frac{2E\,x(1-x)}{k_T^2 + x^2 m_q^2} \approx \frac{2\,\omega}{k_T^2}, \tag{9}$$

where ω is the gluon energy. First are radiated gluons with small longitudinal and large

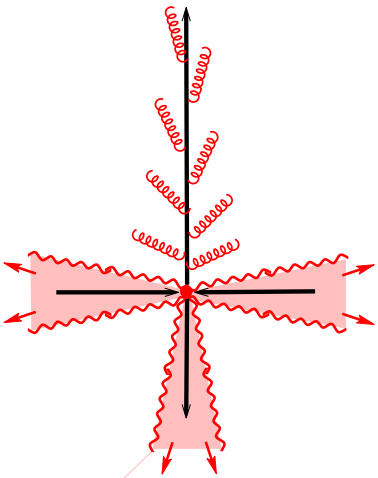

Figure 9. Production of four cones of radiation in a hard parton collision (see the text).

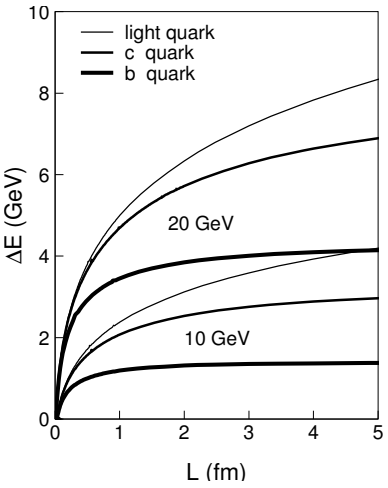

Figure 10. Fractional energy loss by a quark with different initial energies in vacuum vs path length L.

transverse momenta. Energetic gluons with small k_T are radiated at long times.

3.2. Vacuum energy loss

The radiative energy loss is most intensive at the early stage of hadronization, then it slows down. This is confirmed by a direct calculation of the energy radiated over the path length L,

$$\Delta E(L) = E \int_{\Lambda^2}^{Q^2} dk^2 \int_0^1 dx\, x\, \frac{dn_g}{dx\, dk^2} \Theta(L - l_c) \tag{10}$$

where

$$\frac{dn_g}{dx\, dk^2} = \frac{2\alpha_s(k^2)}{3\pi\, x}\, \frac{k^2[1 + (1-x)^2]}{[k^2 + x^2 m_q^2]^2} \tag{11}$$

This expression shows that gluon radiation is subject to a dead-cone effect: gluons with $k^2 < x^2 m_q^2$ are suppressed. Heavy quarks radiate less energy than the light ones [22].

Besides, gluon radiation is suppressed by another dead cone effect: soft gluons cannot be radiated at short path length, since the high-p_T parton is lacking its color field, which was shaken off in the forward direction,

$$k^2 > \frac{2Ex(1-x)}{L} - x^2 m_q^2 \,. \tag{12}$$

This is why heavy and light quarks at the early stage radiate with similar rates, up to short length scale [23]

$$L \lesssim \frac{Ex(1-x)}{x^2 m_q^2} \,. \tag{13}$$

Since the rate of energy dissipation is especially large at the early stage, the parton may lose an essential fraction of its initial energy within a short time interval after the hard collision. Indeed the fractional energy loss depicted in Fig. 11 as function of path length shows that a high-p_T quark loses 40% of the total radiated energy during the first 1fm.

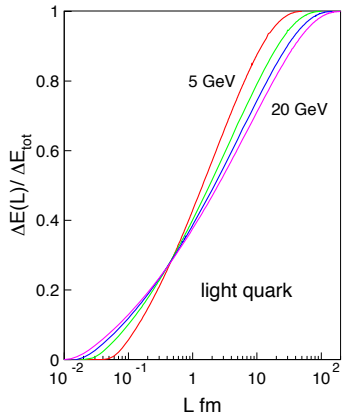

Figure 11. Fractional energy loss by a quark with different initial energies in vacuum vs path length L.

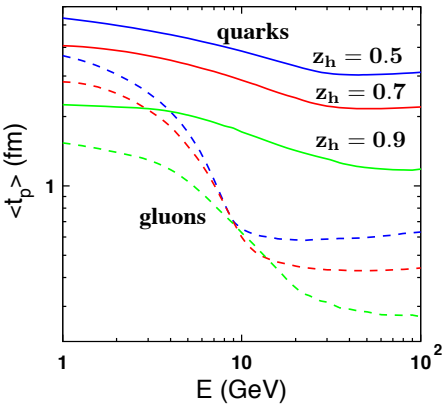

Figure 12. The mean production length vs energy of jets initiated by quarks (solid curves) and gluons (dashed curves). In both cases $z_h = 0.5,\ 0.7,\ 0.9$ (from top to bottom).

This means that Energy conservation restricts the time scale of hadron production. Namely, a hadron with large fractional momentum z_h should be produced at a short time scale, otherwise too much energy will be radiated, and production of the hadron becomes impossible [24, 25, 26]. Notice that in a high-p_T hadron production the large values of z_h are favored by the steeply falling transverse momentum spectrum of quarks convoluted with the fragmentations function [26, 27, 28].

In fact the energy restrictions make the dissipation of energy for a given z_h somewhat slower than it follows from Eq. (10) and is depicted in Figs. 10, because radiation of gluons with fractional momenta larger than $1-z_h$ is forbidden by energy conservation [24, 29]. On the other hand, a ban for radiation of gluons with energy $\omega > (1-z_h)E$ in (10), leads to the Sudakov type suppression factor [25, 29],

$$S(L, z_h) = \exp\left[-\langle n_g(L, z_h)\rangle\right] , \tag{14}$$

where $\langle n_g(L, z_h)\rangle$ is the mean number of nonradiated gluons during propagation over the distance L,

$$\langle n_g(L, z_h)\rangle = \int\limits_{1/Q}^{l_{max}} dl \int\limits_{(2El)^{-1}}^{1} d\alpha \, \frac{dn_g}{dl d\alpha} \, \Theta\left(\alpha + \frac{1-\alpha}{2lE} - 1 + z_h\right) . \tag{15}$$

Here α is the fractional light-cone momentum of a radiated gluon; $l_{max} = \min\{L,\ E/2\lambda^2\}$, and λ is the soft cutoff for transverse momenta of gluons, fixed in [29] at $\lambda = 0.7\,\mathrm{GeV}$. The step function in (15) takes care of energy conservation.

Combination of these two effects, vacuum energy loss and Sudakov suppression, leads to a rather short production length, which slightly varies with jet energy and virtuality. The resulting production length distribution for quark jets with maximal virtuality $Q = p_T/z_h = E$ is depicted in Fig. 12 as function of jet energy [29, 27, 28]. Several examples for quark jets are depicted by solid curves. The mean production length for gluon jets should be shorter, because the more intensive vacuum energy loss and a stronger Sudakov suppression act in the same direction, making the $\langle l_p\rangle$ shorter. The results for gluon jets are shown in Fig. 12 by dashed curves. We see that the mean production length is rather short, and is slowly decreasing with energy (i.e. with the hadron p_T). Therefore, a colorless dipole, which does not lose energy anymore and

later develops the wave function of the detected hadron, is produced at the early stage of jet development and attenuates in the medium. This, rather than induced energy loss, may be the main source of the observed suppression of high-p_T hadrons produced in AA collisions.

3.3. Attenuation of high-p_T hadrons in a hot medium

The transverse size of a colorless dipole fluctuates during its propagation through a medium, and the attenuation rate is varying. The way to describe this process is the path-integral method, summing up all possible trajectories of the dipole constituents [30, 3, 4]. The imaginary part of the light-cone potential, responsible for absorption, is controlled by the transport coefficient $\hat{q}$, which is defined as the rate of transverse momentum broadening of a parton propagating through the medium. The dependence of $\hat{q}$ on transverse coordinate and time passed after the hard collision is usually modeled as [31],

$$\hat{q}(l,\vec{b},\vec{\tau}) = \frac{\hat{q}_0\, l_0}{l}\,\frac{n_{part}(\vec{b},\vec{\tau})}{n_{part}(0,0)}\,\Theta(l-l_0), \tag{16}$$

where $\vec{b}$ is the impact parameter of nuclear collision, $\vec{\tau}$ is the impact parameter of the hard parton-parton collision relative to the center of one of the nuclei, $n_{part}(\vec{b},\vec{\tau})$ is the number of participants, and $\hat{q}_0$ is the rate of broadening of a quark propagating in the maximal medium density produced at impact parameter $\tau = 0$ in central collisions ($b = 0$) at the time $t = t_0 = l_0$ after the collision. The corresponding transport coefficient for gluons should be 9/4 bigger. The equilibration time t_0 is model dependent. The results are not very sensitive to it, so it is fixed it at $t_0 = l_0 = 0.5\,\mathrm{fm}$.

$$R_{AB}(\vec{b},p_T) = \frac{\int d^2\tau\, T_A(\tau)T_B(\vec{b}-\vec{\tau})\int\limits_0^{2\pi}\frac{d\phi}{2\pi}\left|\int\limits_0^1 d\alpha\int d^2r_1 d^2r_2\,\Psi_h^\dagger(\vec{r}_2,\alpha)G_{\bar{q}q}(l_1,\vec{r}_1;l_2,\vec{r}_2)\Psi_{in}(\vec{r}_1,\alpha)\right|^2}{T_{AB}(b)\left|\int\limits_0^1 d\alpha\int d^2r\,\Psi_h^\dagger(\vec{r}_2,\alpha)\Psi_{in}(\vec{r}_1,\alpha)\right|^2}. \tag{17}$$

Here $G_{\bar{q}q}(l_1,\vec{r}_1;l_2,\vec{r}_2)$ is the Green function describing proparagion of a $\bar{q}q$ dipole between the longitudinal coordinates (in the medium rest frame) l_1 and l_2 having the initial and final transverse separations $\vec{r}_{1,2}$; Ψ_{in} and Ψ_h are the light-cone distribution functions of the initial and final (the hadron) dipoles; α is the fractional light-cone momentum; $T_{AB} = \int d^2\tau\, T_A(b)T_B(\vec{b}-\vec{\tau})$; ϕ is the azimuthal angle of the dipole trajectory in impact parameter plane, relative to the impact vector $\vec{b}$ of the collision. The imaginary part of the light-cone potential controlling the solution for the Green function is proportional to the transport coefficient [27, 28] $\hat{q}(l,\vec{b},\vec{\tau})$ along the trajectory, Eq. (16).

The results of calulation [28] at $\sqrt{s} = 2.76\,\mathrm{TeV}$ with $\hat{q}_0 = 2\,\mathrm{GeV}^2/\mathrm{fm}$ are plotted in Fig. 13 by dashed curve in comparison with data from the ALICE [32] and CMS [33, 34] experiments. While $\hat{q}_0$ controls the normalization of $R_{AA}(p_T)$, the shape of the p_T-dependence is parameter free and well reproduces the data.

With the fixed value of the parameter $\hat{q}_0$ one also reproduces well the p_T-dependence of R_{AA} observed at different centralities of collision (see detailes in [28]).

Similar calculations performed at $\sqrt{s} = 200\,\mathrm{GeV}$ with $\hat{q}_0 = 1.6\,\mathrm{GeV}^2/\mathrm{fm}$ are depicted in Fig. 15 by dashed curve. Data do not support such a steep rise of R_{AA} with p_T.

3.4. Azimuthal asymmetry

As far as the produced hadron suppression correlates with the path of the dipole in the hot absorptive medium, this leads to an azimuthal asymmetry for hadron production from the

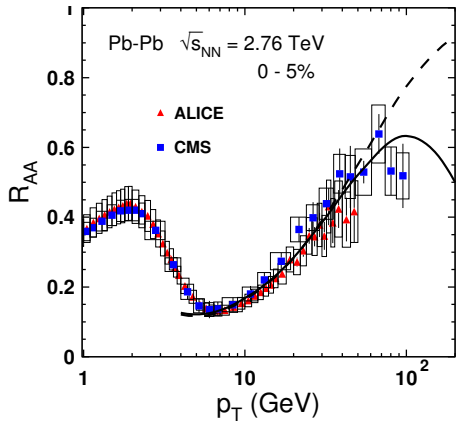

Figure 13. The suppression factor R_{AA} for central lead-lead collisions at $\sqrt{s} = 2.76\,\text{TeV}$. The dashed line is calculated within the path-integral approach [28] with the transport coefficient Eq. (16), where the adjusted parameter $\hat{q}_0 = 2\,\text{GeV}^2/\text{fm}$. The solid curve also includes the effects of initial state interactions in nuclear collisions [16, 19]. Data are from the ALICE [32] and CMS [33, 34] experiments.

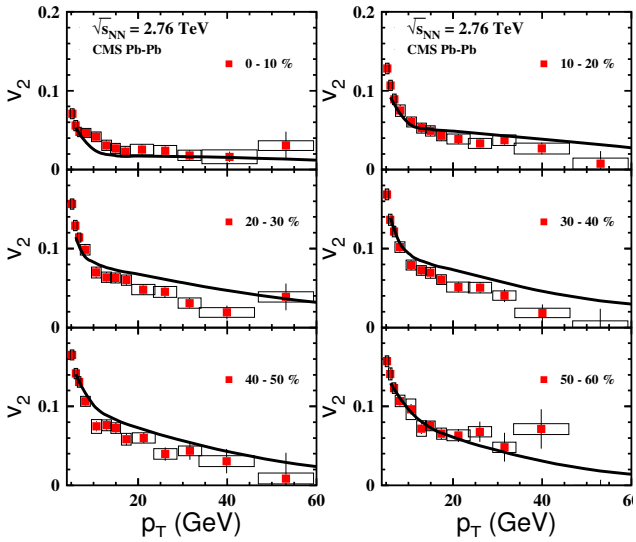

Figure 14. CMS data [35] for azimuthal anisotropy, v_2, vs p_T for charge hadron production in lead-lead collisions at mid rapidity, at $\sqrt{s} = 2.76$ TeV and at different centralities indicated in the figure. The curves present the results of calculation with Eq. (18) and $\hat{q}_0 = 2\,\text{GeV}^2/\text{fm}$ [28].

almond-shaped overlap in a non-central collision of nuclei. It can be calculated similarly to Eq. (17),

$$v_2(p_T, b) = \frac{\int d^2\tau\, T_A(\tau) T_B(\vec{b}-\vec{\tau}) \int_0^{2\pi} d\phi \cos(2\phi) \left| \int_0^\infty dr\, r\, \Psi_h(r) G_{\bar{q}q}(0,0;l_{max},r) \right|^2}{\int d^2\tau\, T_A(\tau) T_B(\vec{b}-\vec{\tau}) \int_0^{2\pi} d\phi \left| \int_0^\infty dr\, r\, \Psi_h(r)\, G_{\bar{q}q}(0,0;l_{max},r) \right|^2}. \qquad (18)$$

Comparison with the data, performing another sensitive test of the model, is presented in FIg. 14. The agreement at large p_T is rather good.

3.5. Energy deficit at high p_T

Similar to the effects of energy deficit observed at large p_T in dA collisions at RHIC (Fig. 8), production of hadrons at large x_T should also be suppressed. At $\sqrt{s} = 5\,\text{TeV}$ such an additional suppression becomes significant at rather large $p_T \gtrsim 100\,\text{GeV}$, as is shown by solid curve in Fig. 13. The points at largest measured p_T indeed seem to deviate from the dashed curve.

Naturally, the lower is the collision energy, the earlier onsets the effect of energy deficit, because it scales in x_T. The results at $\sqrt{s} = 200\,\text{GeV}$ including the energy loss corrections are plotted Fig. 15 by solid curve in comparison with data. Apparently, the additional suppression caused by energy deficit improves agreement with the data.

Even a stronger effect of energy loss is expected at lower collision energies. Our predictions at $\sqrt{s} = 62\,\text{GeV}$ with $\hat{q}_0 = 1.2\,\text{GeV}^2/\text{fm}$ corrected for energy deficit are compared with data at difference centralities in Fig. 16. We see that the energy loss corrections are so strong that cause a falling, rather than rising, p_T-dependence of R_{AA}.

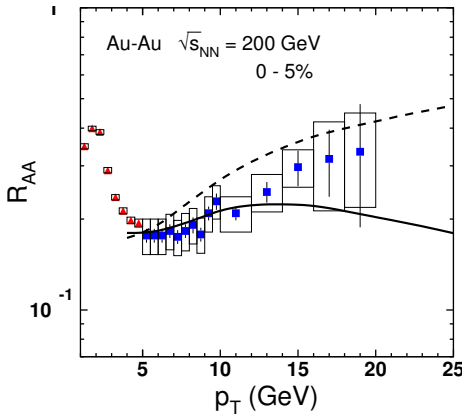

Figure 15. Nuclear attenuation factor $R_{AA}(p_T)$ for neutral pions produced in central gold-gold collisions at $\sqrt{s} = 200$ GeV. The solid and dashed line are calculated with or without ISI corrections. PHENIX data are from [36] (triangles)

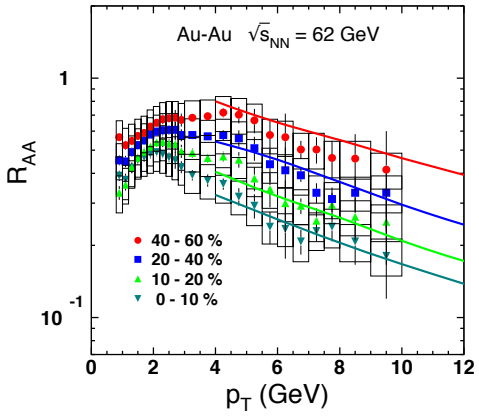

Figure 16. Centrality dependence of the suppression factor $R_{AA}(p_T, b)$ in gold-gold collisions at $\sqrt{s} = 62.4$ GeV [36]. The curves are calculated including FSI attenuation of dipoles in the dense medium and the ISI energy loss effects.

4. Summary

Summarizing, in this note we investigated the impact of energy conservation in several high-energy processes involving nuclei. In many instances we observed significant effects:

- The color-dipole description of high-p_T hadron production is tested on the Cronin effect at the fixed target and collider energies. The description is found to be quite successful and having a strong predictive power. In particular, the magnitude of the Cronin enhancement was successfully predicted prior the measurements at RHIC and LHC.
- Energy conservation significantly suppresses cross sections upon approaching the kinematic bounds, at large x_L and/or at large x_T. The presented parameter-free calculations well explain the observed suppression seen in data from RHIC for hadron production at forward rapidities, or at the mid-rapidity, but very large p_T. Predictions for the energy of LHC are presented as well.
- Inclusive production of high-p_T hadrons in heavy ion collision is subject to final state interactions with the dense quark-gluon medium created in the collision. The popular energy loss interpretation, based on the unjustified assumption of a long hadronization length, conflicts with energy conservation because of the intensive energy dissipation by a highly virtual parton produced in a high-p_T process. The inclusively detected hadron, having a large mean fractional momentum $\langle z_h \rangle$, cannot be produced on a long time scale and respect energy conservation. As far as the production of a colorless dipole occurs on a short length scale, the dipole attenuation and color transparency become the driving dynamics of the observed hadron suppression. The path-integral technique for calculation of the dipole attenuation results in a successful description of available data for nuclear quenching of high$-p_T$ hadrons produced in AA collisions at the energies of RHIC and LHC. The parameter, the transport coefficient $\hat{q}$, characterizing the interaction with the medium, is found at a reasonable magnitude, expected in the theory, while the energy loss scenario has been always suffering of a gross over-evaluation of this parameter. The observed azimuthal asymmetry at RHIC and LHC is well explained as well, without any further adjustment.
- Energy conservation and energy sharing restrictions produce an additional suppression in the case of heavy ion collisions as well. These effects are found especially strong at the

energies of RHIC $\sqrt{s} \leq 200\,\text{GeV}$, but also are expected at LHC, either beyond the currently measured range of p_T, or at forward rapidities.

Acknowledgments
This work was supported in part by Fondecyt (Chile) grants 1130543, 1130549, 1100287, and by Conicyt-DFG grant No. RE 3513/1-1. The work of J.N. was partially supported by the grant 13-20841S of the Czech Science Foundation (GAČR), by the Grant MSMT LG13031, by the Slovak Research and Development Agency APVV-0050-11 and by the Slovak Funding Agency, Grant 2/0020/14.

References
[1] Kopeliovich B Z, Nemchik J, Schäfer A and Tarasov A V 2002 *Phys. Rev. Lett.* **88** 232303
[2] Johnson M B, Kopeliovich B Z and Tarasov A V 2001 *Phys. Rev.* C **63** 035203
[3] Kopeliovich B Z, Tarasov A V and Schäfer A 1999 *Phys. Rev.* C **59** 1609
[4] Kopeliovich B Z, Schäfer A and Tarasov A V 2000 *Phys. Rev.* D **62** 054022
[5] Kopeliovich B Z, Potashnikova I K, Povh B and Schmidt I 2007 *Phys. Rev.* D **76** 094020
[6] Di Giacomo A and Panagopoulos H 1992 *Phys. Lett.* B **285** 133
[7] Golec-Biernat K J and Wüsthoff M 1998, *Phys. Rev.* D **59** 014017
[8] Kimber M A , Martin A D and Ryskin M G 2001 *Phys. Rev.* D **63** 114027
[9] Martin A D, Ryskin M G and Watt G 2010 *Eur. Phys. J.* C **66** 163
[10] Kharzeev D, Levin E and McLerran L 2003 *Phys. Lett.* B **561** 93
[11] Gribov V N 1969 *Sov. Phys. JETP* **29** 483 [*Zh. Eksp. Teor. Fiz.* **56** 892].
[12] Adler S S *et al* [PHENIX Collaboration] 2007 *Phys. Rev. Lett.* **98** 172302
[13] Abelev B *et al.* [ALICE Collaboration] 2013 *Phys. Rev. Lett.* **110**, 082302
[14] de Florian D and Sassot R 2004 *Phys. Rev.* D **69** 074028
[15] Albacete J L *et al.* 2013 *Int. J. Mod. Phys.* E **22** 1330007
[16] Kopeliovich B Z, Nemchik J, Potashnikova I K, Johnson M B and Schmidt I 2005 *Nucl. Phys.* B **146** 171
[17] Arsene I *et al* [BRAHMS Collaboration] 2004 *Phys. Rev. Lett.* **93** 242303
[18] Adams J *et al* [STAR Collaboration] 2006 *Phys. Rev. Lett.* **97** 152302
[19] Kopeliovich B Z, Nemchik J 2011 *J. Phys. G* **38** 043101
[20] Kharzeev D, Kovchegov Y V and Tuchin K 2004 *Phys. Lett.* B **599** 23
[21] Boimska B [NA49 Collaboration] 2004 *Ph.D. Dissertation* **CERN-THESIS-2004-035**
[22] Dokshitzer Y L and Kharzeev D E 2001 *Phys. Lett.* B **519** 199
[23] Kopeliovich B Z, Potashnikova I K and Schmidt I 2007 *Phys. Rev.* C **82** 037901
[24] Kopeliovich B Z, Nemchik J and Predazzi E 1996 *Proceedings of the workshop on Future Physics at HERA* ed. by Ingelman G, De Roeck A and Klanner R *DESY 1995/1996* v.2 1038
[25] Kopeliovich B Z, Nemchik J, Predazzi E and Hayashigaki A 2004 *Nucl. Phys.* A **740** 211
[26] Kopeliovich B Z, Nemchik J and Schmidt I 2007 *Nucl. Phys.* A **782** 224
[27] Kopeliovich B Z, Potashnikova I K and Schmidt I 2011 *Phys. Rev.* C **83**, 037901
[28] Kopeliovich B Z, Nemchik J, Potashnikova I K and Schmidt I 2012 *Phys. Rev.* C **86** 054904
[29] Kopeliovich B Z, Pirner H J, Potashnikova I K and Schmidt I 2008 *Phys. Lett.* B **662** 117
[30] Kopeliovich B Z and Zakharov B G 1991 *Phys. Rev.* D **44** 3466
[31] Chen X F, Greiner C, Wang E, Wang X N and Xu Z 2010 *Phys. Rev.* C **81** 064908
[32] Abelev B *et al.* [The ALICE Collaboration] 2013 *Phys. Lett.* B **720** 52
[33] Lee Y J (for the CMS Collaboration) 2011 *J. Phys. G* **38** 124015
[34] A. S. Yoon A S (for the CMS Collaboration) 2011 *J. Phys. G* **38** 124116
[35] Chatrchyan S *et al.* [CMS Collaboration] 2012 *Phys. Rev. Lett.* **109** 022301
[36] Adare A *et al.* [PHENIX Collaboration] 2013 *Phys. Rev.* C **87** 034911
[37] M. L. Purschke M L (for the PHENIX Collaboration) 2011 *J. Phys. G* **38** 124016
[38] PHENIX Collaboration 2012 preliminary data posted at www.phenix.bnl.gov/WWW/plots/show_plot.php?editkey=p1118